The Plant Cell, Vol. 25: 4014–4027, October 2013, www.plantcell.org © 2013 American Society of Plant Biologists. All rights reserved.

The Evolutionarily Conserved Iron-Sulfur Protein INDH Is Required for Complex I Assembly and Mitochondrial Translation in *Arabidopsis*[C][W][OPEN]

Mateusz M. Wydro,[a] Pia Sharma,[a] Jonathan M. Foster,[a] Katrine Bych,[a] Etienne H. Meyer,[b] and Janneke Balk[a,c,d,1]

[a] Department of Plant Sciences, University of Cambridge, Cambridge CB2 3EA, United Kingdom
[b] Max Planck Institute for Molecular Plant Physiology, D-14476 Potsdam-Golm, Germany
[c] Department of Biological Chemistry, John Innes Centre, Norwich NR4 7UH, United Kingdom
[d] School of Biological Sciences, University of East Anglia, Norwich NR4 7TJ, United Kingdom

The assembly of respiratory complexes is a multistep process, requiring coordinate expression of mitochondrial and nuclear genes and cofactor biosynthesis. We functionally characterized the iron-sulfur protein required for NADH dehydrogenase (INDH) in the model plant *Arabidopsis thaliana*. An *indh* knockout mutant lacked complex I but had low levels of a 650-kD assembly intermediate, similar to mutations in the homologous NUBPL (nucleotide binding protein-like) in *Homo sapiens*. However, heterozygous *indh*/+ mutants displayed unusual phenotypes during gametogenesis and resembled mutants in mitochondrial translation more than mutants in complex I. Gradually increased expression of *INDH* in *indh* knockout plants revealed a significant delay in reassembly of complex I, suggesting an indirect role for INDH in the assembly process. Depletion of INDH protein was associated with decreased ^{35}S-Met labeling of translation products in isolated mitochondria, whereas the steady state levels of several mitochondrial transcripts were increased. Mitochondrially encoded proteins were differentially affected, with near normal levels of cytochrome *c* oxidase subunit2 and Nad7 but little Nad6 protein in the *indh* mutant. These data suggest that INDH has a primary role in mitochondrial translation that underlies its role in complex I assembly.

INTRODUCTION

Mitochondria are the powerhouses of the cell, generating ATP through oxidative phosphorylation (OXPHOS) mediated by a series of large membrane-bound protein complexes I to V. The majority of mitochondrial proteins are encoded in the nuclear genome and imported into the organelle, but ~10 to 50 proteins are encoded by the remnant mitochondrial genome in most eukaryotes. The dual-genetic origin adds an extra layer of complexity to the assembly of complexes I and III to V. Mitochondrial genes need to be faithfully decoded, requiring a complete expression system in the mitochondria. The subunits then need to be assembled in a coordinate manner with the imported, nuclear-encoded proteins and specific cofactors.

Respiratory complex I, NADH:ubiquinone oxidoreductase, oxidizes NADH, linking electron flow to proton pumping across the mitochondrial inner membrane (Brandt, 2006). The large ~1 MD protein complex has an L-shape, consisting of a hydrophilic arm, known as the peripheral arm, protruding in the mitochondrial matrix, as well as a hydrophobic arm embedded in the inner mitochondrial membrane. The peripheral arm carries out the oxidation of NADH and transfers the electrons to ubiquinone over a chain of seven iron-sulfur (Fe-S) clusters. The membrane arm pumps protons from the matrix to the intermembrane space using a suggested piston mechanism (Zickermann et al., 2009; Efremov and Sazanov, 2011). Of the ≥40 subunits, 7 are encoded by the mitochondrial genome in most eukaryotes and are part of the hydrophobic membrane arm, including NADH dehydrogenase 1 (ND1), ND2, ND3, ND4, ND4L, ND5, and ND6. In plants, an additional two subunits of the peripheral arm are also mitochondrially encoded, which are NADH dehydrogenase 7 and 9 (Nad7 and Nad9), homologs of the 49-kD and 30-kD subunits in bovine, respectively. The complex is assembled in a modular way with the help of at least 10 assembly factors (Meyer et al., 2011; Hoefs et al., 2012; Mimaki et al., 2012). Complex I in plants follows a similar assembly pattern, except that it builds on the assembly of the plant-specific carbonic anhydrase module as an early step (Meyer et al., 2011; Li et al., 2013). It is not yet known whether any of the mammalian assembly factors are conserved in plants.

Given its size and complex structure, it is perhaps unsurprising that defects in complex I function are commonly found. The majority of human OXPHOS disorders are a result of complex I deficiency, caused by mutations in one of the 44 structural subunits, in one of the assembly factors, or in mitochondrial gene expression (Tucker et al., 2011; Hoefs et al., 2012). Some cases of complex I deficiency in humans are caused by mutation of a specific mitochondrial tRNA (Calvo et al., 2010; Swalwell et al., 2011), whereas a growing number of nuclear mutants are being described that affect splicing or editing

[1] Address correspondence to janneke.balk@jic.ac.uk.
The author responsible for distribution of materials integral to the findings presented in this article in accordance with the policy described in the Instructions for Authors (www.plantcell.org) is: Janneke Balk (janneke.balk@jic.ac.uk).
[C] Some figures in this article are displayed in color online but in black and white in the print edition.
[W] Online version contains Web-only data.
[OPEN] Articles can be viewed online without a subscription.
www.plantcell.org/cgi/doi/10.1105/tpc.113.117283

of the mitochondrial *nad* transcripts in plants (Colas de Francs-Small and Small, 2013).

An assembly factor called IND1 (for iron-sulfur protein required for NADH dehydrogenase) was recently identified in the yeast *Yarrowia lipolytica* (Bych et al., 2008b). IND1 has a similar phylogenetic distribution to complex I, although this association was not uncovered in previous bioinformatics and systems studies (Gabaldón et al., 2005; Pagliarini et al., 2008). The 30-kD protein belongs to a subfamily of P-loop NTPases involved in Fe-S protein biogenesis (Bych et al., 2008a; Lill, 2009). The Ind1 homologs are classified based on a predicted mitochondrial targeting peptide and are 30% identical (50% similar) in amino acid sequence (see Supplemental Figure 1 online). Deletion of *IND1* in *Y.* led to an 80% decrease in complex I levels and activity, but no obvious effect on other respiratory complexes or other Fe-S proteins during vegetative growth. The Ind1 protein has a conserved CxxC motif in the C terminus and binds a labile Fe-S cluster. We showed that the cluster could be transferred to another single-subunit Fe-S protein in vitro, but whether it is transferred to Fe-S subunits of complex I in vivo has not yet been technically possible to demonstrate. The human homolog of *IND1*, *Nucleotide Binding Protein 1-Like (NUBPL)*, is also specifically required for complex I assembly as shown using an RNAi approach in HeLa cells (Sheftel et al., 2009). Moreover, mutations in *NUBPL* have been linked to complex I deficiency in patients with mitochondrial disease (Calvo et al., 2010; Tenisch et al., 2012; Kevelam et al., 2013). Of the cases described thus far, one *NUBPL* allele is a null allele, whereas the other allele has both a missense mutation (G56R) and a branch-site mutation leading to a frameshift after Gly272 (Tucker et al., 2012; Kevelam et al., 2013). Reconstruction of the altered C terminus in the *Y. lipolytica* Ind1 protein showed that the mutant protein is instable (Wydro and Balk, 2013). The branch-site mutation is found in 1.2% (7 of 751, www.ensembl.org) of the European population, but how this affects individuals is currently unknown because little is yet known about IND1 and its homologs.

To learn more about the function of *IND1*, we studied mutant alleles of the homologous *INDH* gene (*At4G19540*) in the model plant *Arabidopsis thaliana*, in which the gene was first described but has thus far remained uncharacterized (Lezhneva et al., 2004; Bych et al., 2008a). Compared with previous investigations in *Y. lipolytica* and human cell lines, both vegetative cells, the plant model system allowed for a detailed analysis of mutant phenotypes during reproductive development. In addition, gradual "switch-on" of *INDH* expression in a knockout mutant helped to unravel primary from secondary phenotypes. Together, our results indicate that INDH has a primary role in mitochondrial translation, associated with gametogenesis defects in the heterozygote, that indirectly but specifically affects the assembly of complex I.

RESULTS

Arabidopsis INDH Is a Mitochondrial Protein of Low Abundance

The INDH protein sequence has a high probability for mitochondrial targeting according to prediction programs (TargetP, Predotar, iPSORT) and was recently found by mass spectrometry in purified mitochondria (Klodmann et al., 2011). To confirm its cellular localization experimentally, antibodies were raised against recombinant INDH and used to detect their target in total cell extract and purified organelles from wild-type seedlings. A specific immunolabeling signal of 30 kD was observed in the mitochondrial fraction, but not in chloroplasts (Figure 1A). No signal was detected in an equal amount of total protein extract, but this might be a result of the low abundance of INDH, which was estimated to be less than 0.1% of total mitochondrial protein, based on comparison with purified INDH.

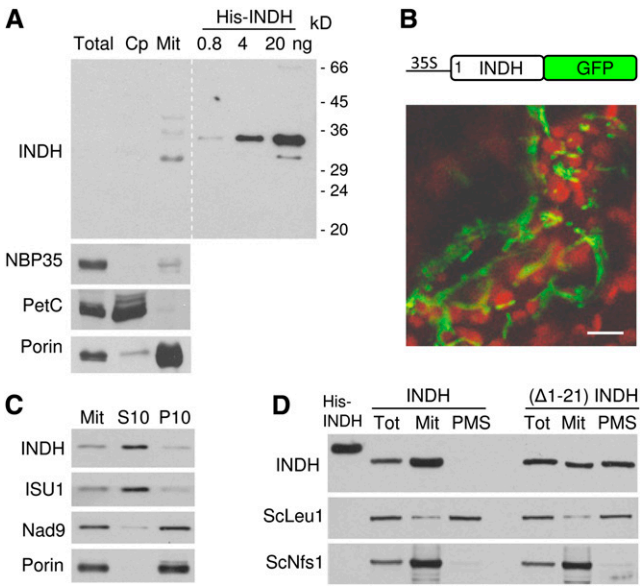

Figure 1. INDH Is a Protein of Low Abundance in the Mitochondria.

(A) Immunolocalization of endogenous INDH. Equal amounts of protein (30 μg) from total leaf extract, gradient-purified chloroplasts (Cp), or mitochondria (Mit) were separated by SDS-PAGE, blotted, and labeled with antibodies against the indicated proteins. NBP35 served as a cytosolic marker protein, PetC (Rieske) as a chloroplast marker, and porin as a mitochondrial marker. Known amounts of purified His-tagged INDH were included to assess the abundance of endogenous INDH.

(B) Transient expression of *INDH* fused to *GFP* under the control of the CaMV 35S promoter in epidermal leaf cells (green). Autofluorescence of chloroplasts is red. Bar = 5 μm.

(C) INDH is a soluble matrix protein. Purified mitochondria were subjected to three cycles of freeze-thawing and separated into supernatant (S10) and pellet (P10) by centrifugation at 10,000*g* for 10 min. Equal amounts (10 μg) of protein were separated by SDS-PAGE, blotted, and labeled with antibodies against INDH, ISU1 (a soluble matrix protein), Nad9 (a subunit of respiratory complex I), and porin (an integral membrane protein).

(D) The first 21 amino acids of INDH are important for mitochondrial targeting. The full-length coding sequence of *INDH*, or *INDH* lacking the first 21 codons, was cloned into the pRS416 vector and expressed in the yeast *S. cerevisiae*. Cells were fractionated into total cell extract (Tot), mitochondria (Mit), and postmitochondrial supernatant (PMS) by differential centrifugation. Equal amounts of protein (10 μg) were subjected to immunoblotting with antibodies against INDH, and against the *S. cerevisiae* proteins Leu1 and Nfs1 as cytosolic and mitochondrial markers, respectively.

To consolidate the fractionation and immunolabeling results, the cDNA of *INDH* was cloned in frame with green fluorescent protein (*GFP*) under the control of the cauliflower mosaic virus (CaMV) 35S promoter and transiently expressed in *Arabidopsis* epidermal cells. Fluorescence was detected in a punctate pattern surrounding the chloroplasts, characteristic of mitochondria (Figure 1B).

To establish in which mitochondrial subcompartment INDH resides, mitochondria were separated in a soluble matrix fraction (S10) and a membrane pellet fraction (P10) and subjected to immunoblot analysis. INDH was enriched in the soluble fraction, similar to the Fe-S scaffold protein Iron-Sulfur cluster U (ISU1) Figure 1C). By contrast, the Nad9 subunit of complex I and the integral membrane protein porin were, as expected, enriched in the membrane fraction.

Based on the electrophoretic mobility of INDH (Figure 1A) and the calculated molecular mass of full-length protein, the N-terminal targeting sequence is predicted to be relatively short, with a cleavage site after Tyr22 (TargetP). Indeed, removal of the first 21 codons severely compromised import of INDH into mitochondria in the yeast *Saccharomyces cerevisiae* (Figure 1D). Whereas expression of full-length INDH targeted the protein exclusively to the mitochondrial fraction (Mit), ~50% of the truncated protein was found in the cytosolic fraction (postmitochondrial supernatant).

In summary, these data show that INDH is localized in the mitochondrial matrix, to which it is directed by a canonical N-terminal–targeting peptide.

The *INDH* Gene Is Important for Early Vegetative Growth

To study the function of INDH, we searched the *Arabidopsis* stock centers for insertion mutants. Only one insertion line was found: GK_956A05 in the Gabi-Kat collection. In this line, the T-DNA is inserted in the seventh exon (Figure 2A), 20 bp upstream of the codons for the conserved CxxC motif. T3 seed from a heterozygous plant was germinated on basic salt medium and 10-d-old seedlings were analyzed by PCR for the presence of the T-DNA insertion and wild-type allele. Heterozygous and wild-type seedlings segregated in a ~1:1 ratio and were similar in appearance, but no homozygous *indh* mutants were found (Figures 2B, left panels, and 2C; see Supplemental Tables 1 and 2A online). The segregation ratio was confirmed by scoring seedlings for resistance to sulfadiazine, the selection marker contained within the T-DNA, which was 142:129 (resistant: sensitive). The ratio is clearly different from the Mendelian 2:1 ratio expected for an essential gene.

Upon closer inspection, we noticed that many seeds failed to germinate or that seedlings were arrested in early growth. Therefore, T3 seeds were planted on medium with 1% (w/v) Suc. More than 95% of the seed germinated, 19% of which (175 of 923) was severely delayed in vegetative development (Figure 2C). Small seedlings were analyzed by PCR and found to be homozygous for *indh* (Figure 2B, right panels) and lacking INDH protein (see below). PCR analysis further showed that of 20 normal-sized seedlings, 10 were heterozygous and 10 were wild type. Therefore, on Suc medium, the *indh* knockout allele segregated 0.7:1:1 (*indh*:heterozygous:wild type). The *indh* seedlings were transferred to soil and grown under long-day conditions. They bolted after ~6 weeks and produced seeds after 9 weeks, compared with 4 and 6 weeks, respectively, in the wild type. The *indh* inflorescences were highly branched and reached only half the height of wild-type plants (Figure 2D).

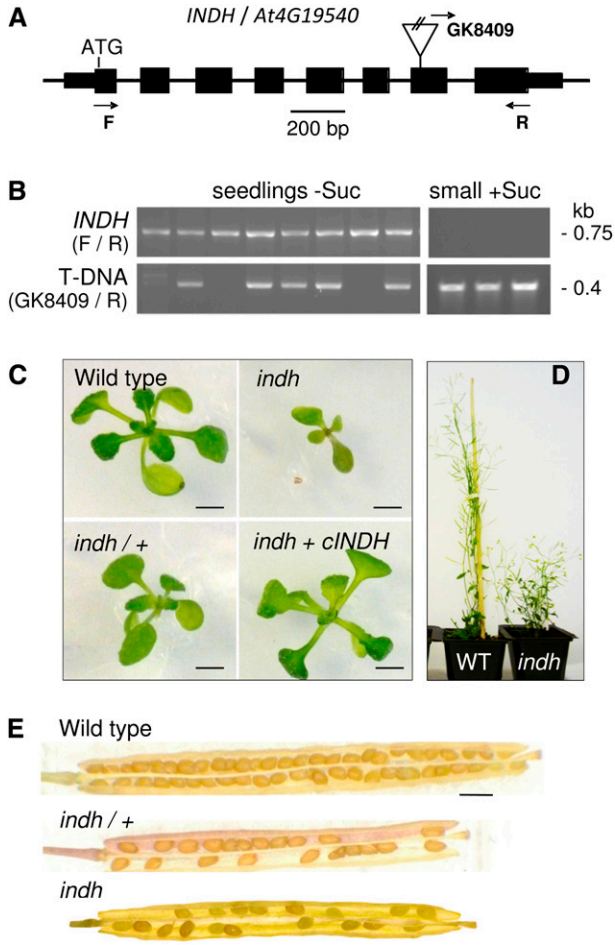

Figure 2. *INDH* Is Important for Early Seedling Development and Seed Production.

(A) Gene structure of the *INDH* gene, *AT4G19540*, and the position of the T-DNA insertion (triangle) in line GK_956A05. Primers are indicated by arrows.

(B) PCR analysis for segregation of wild type (*INDH*) and mutant alleles (T-DNA) from a heterozygous *indh*/+ individual. Seedlings segregated ~1:1 in wild type to heterozygous on basic salt medium (left eight lanes). Late developing, small seedlings isolated from medium with 1% Suc were homozygous for the T-DNA insertion in *INDH* (*indh* mutant, right three lanes). The primer combination used for each PCR is indicated in brackets, and the positions of the primers in the *INDH* gene are indicated in **(A)**.

(C) Growth of 14-d-old seedlings of wild type, homozygous *indh*, heterozygous *indh*/+, and *indh* complemented with the cDNA sequence of wild-type *INDH* under the control of the CaMV 35S promoter. Seeds were planted on 1/2 Murashige and Skoog medium with 1% (w/v) Suc. Bar = 2 mm.

(D) Eight-week-old plants grown under long-day conditions. WT, wild type.

(E) Opened silique from the wild type **(top),** heterozygous *indh*/+ **(middle)**, and homozygous *indh* **(bottom)**. Bar = 1 mm.

[See online article for color version of this figure.]

We also noticed a significant decrease in seed set, both in the heterozygous and homozygous *indh* plants, of ~50% and 30% compared with the wild type, respectively (Figure 2E; see Supplemental Table 1 online). There was no bias for seed set with respect to distance from the stigma, arguing against a defect in pollen tube growth.

Heterozygous *indh*/+ Plants Have Sporophytic Defects in Female and Male Gametophyte Development

To further investigate the unusual segregation ratio of heterozygous *indh*/+, we examined gametophyte development using microscopy. Seeds that failed to develop were small and white, resembling unfertilized ovules (Figure 3A). Inspection of immature siliques showed two sizes of ovules: the larger one contained a developing embryo and the smaller ovules arrested at the stage of a mature embryo sac (Figures 3B to 3D).

Pollen development proceeded normally in *indh*/+ until after meiosis (Figure 3E). At stage 11 (Sanders et al., 1999), the cytoplasm came away from the pollen wall in ~40% of the cells, followed by collapse of the pollen grain. The tapetum tissue in *indh*/+ appeared like that of the wild type and underwent its usual developmental program of cell death (Balk and Leaver, 2001).

The 0.7:1:1 segregation ratio and the observed ovule and pollen abortion prompted us to investigate the inheritance of the *indh* allele from either the male or female heterozygous parent. Reciprocal crosses were performed between *indh*/+ and wild type, and seeds germinated on selective medium. The sulfadiazine-resistance marker present in the T-DNA (*indh* allele) was efficiently transmitted through both the female and male gametophyte with

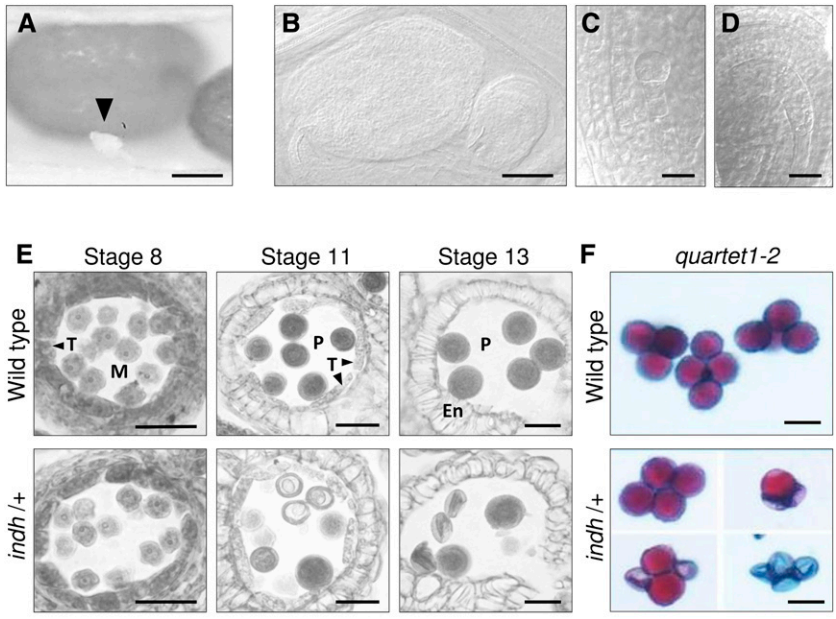

G

Cross (female x male)	F1: Sulfadiazine resistant (R)	F1: Sulfadiazine sensitive (S)	Transmission efficiency (%)
indh/+ x WT	105	109	96%
WT x *indh*/+	217	243	89%
WT x WT	0	113	N/A

Figure 3. Heterozygous *indh*/+ Plants Exhibit Gametogenesis Defects.

(A) Wild-type seed next to an arrested ovule (arrowhead) in the silique of an *indh*/+ plant. Bar = 100 μm.

(B) Ovules of two different sizes in *indh*/+ in immature siliques. Siliques were cleared with Hoyer's solution and imaged with differential interference contrast microscopy, as shown in **(B)** to **(D)**. Bar = 50 μm.

(C) and **(D)** The larger size ovules develop an embryo **(C)**, whereas smaller size ovules contain an embryo sac but fail to further develop **(D)**. Bar = 20 μm.

(E) Pollen development in wild type and *indh*/+ plants. Approximately half of the pollen dies in *indh*/+ with the first visible signs of collapse after meiosis. Thin sections of polyethylene glycol-embedded anthers after histological staining. En, endodermis; M, meiocytes; P, pollen; T, tapetum. Bar = 20 μm.

(F) Segregation of live and dead pollen in *indh*/+ with the *quartet1-2* mutation. The pollen was stained with Alexander's stain, which colored live cells, whereas dead cells were transparent and shrivelled. See Supplemental Figure 2 online for the frequency distribution of the tetrads. Bar = 20 μm.

(G) The *indh* mutant allele is transmitted through both the male and female gametophyte. Transmission efficiency (%) = (#R/#S) × 100. N/A, not applicable; WT, wild type or +/+.

[See online article for color version of this figure.]

96% and 89% efficiency, respectively (Figure 3G). To verify that the sulfadiazine resistance was linked to the transmitted T-DNA, 14 resistant seedlings derived from the crosses were picked randomly and genotyped by PCR. In all of those, the T-DNA insertion in *INDH* was indeed detected. The slightly lower transmission efficiencies are in agreement with the observed ~19% homozygous *indh* segregating from a heterozygous plant on Suc medium (against 25% expected), but it does not explain the 1:1 ratio of heterozygous to wild-type offspring.

To confirm that the collapse of an individual pollen grain was independent of the presence of the *indh* allele, the recessive *quartet1-2* mutation (Francis et al., 2006) was crossed into *indh*/+ for tetrad analysis. The number of collapsed pollen varied from zero to four in the tetrads (Figure 3F), although there was a bias for 2:2 segregation (see Supplemental Figure 2 online). These results indicate that the observed pollen death is caused either by a dominant negative effect of *INDH* disruption in the heterozygote, or by haploinsufficiency in combination with non-Mendelian (cytoplasmic) segregation during gametogenesis. In either case, the collapse of the pollen is a result of a sporophytic defect.

Isolation and Characterization of Fully and Partially Complemented *indh* Mutant Lines

To confirm that the observed phenotypes were attributable to disruption of the *INDH* gene, we complemented the GK_956A05 line with cDNA of wild-type *INDH* (*cINDH*). The distance between the 5′ untranslated region of *INDH* and the 3′ untranslated region of the upstream gene (*AT4G19530*) is only 100 bp, leaving uncertainty about the length of the *INDH* promoter, which could either be short or overlapping with the upstream gene. Therefore, *cINDH* was cloned behind the commonly used CaMV 35S promoter (*35S:cINDH*) in the pBIN vector. In addition, a second construct was made for expression of *cINDH* using the promoter of the *UBIQUITIN11* gene (*UQ11:cINDH*) in pART27, because the 35S promoter is known to be poorly expressed in pollen.

Heterozygous *indh*/+ plants were transformed, and the T1 seeds planted on growth medium with antibiotics to select independent transformants that also carried the *indh* allele (sulfadiazine resistance). Five of 17 plants were homozygous for *indh* and contained the *cINDH* transgene, whereas the other 12 were heterozygous for *indh*, as confirmed by PCR (Figure 4A). The expression of INDH protein was assessed by protein blot analysis. The transgenic INDH protein levels were generally much higher than in the wild type, and were easily detectable in total cell extract (Figure 4B). Vegetative growth in the complemented mutants was like that of the wild type, without any sign of deleterious effects of *INDH* overexpression (Figure 2C; see Supplemental Figure 3 online). Pollen viability was fully restored by expression of *cINDH* from either promoter. However, while seed set was similar to that of the wild type in the *UQ11:cINDH* lines, it was only 70% in the *35S:cINDH*-complemented *indh* lines, compared with 57% in heterozygous *indh*/+ plants grown in parallel (Figures 4C and 4D).

In summary, expression of the wild-type sequence of *INDH* complements both the vegetative and reproductive phenotypes

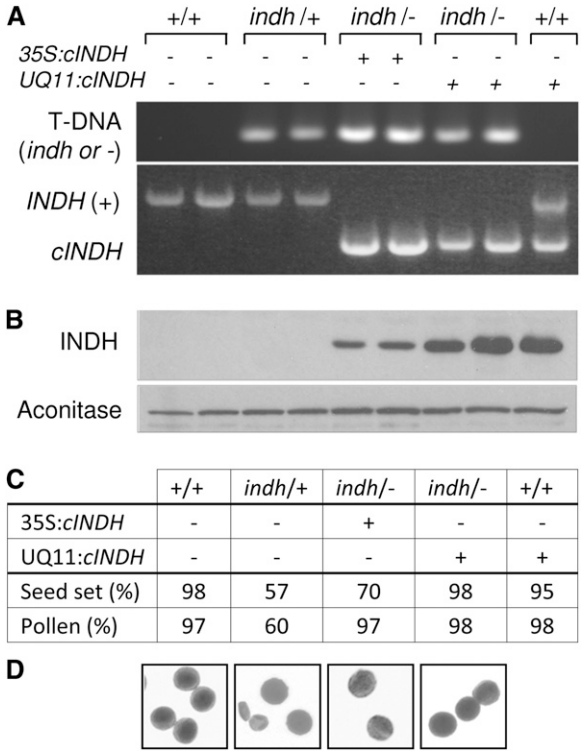

C

	+/+	indh/+	indh/-	indh/-	+/+
35S:*cINDH*	-	-	+	-	-
UQ11:*cINDH*	-	-	-	+	+
Seed set (%)	98	57	70	98	95
Pollen (%)	97	60	97	98	98

D

Figure 4. Complementation of the *indh* Mutant by *cINDH* Transgene Expression.

(A) PCR analysis of wild-type (+/+), heterozygous *indh*/+, and independent T_2 individuals. Specific primers were used to detect the T-DNA insertion in *INDH* (*indh* or −), the wild type allele (*INDH* or +), and the *INDH* transgene derived from cDNA (*cINDH*). *cINDH* expression was under the control of either the CaMV 35S promoter or the *UBIQUITIN11* (*UQ11*) promoter. *cINDH* lacks introns, resulting in a smaller PCR product.
(B) Levels of INDH protein in leaf extract from the same plants as in **(A)**, detected by immunoblot analysis. Antibodies against aconitase were used as a loading control.
(C) Percentage of seed set and pollen viability in the same plant lines as in **(A)**. $n \geq 300$.
(D) Images of pollen from plant lines as in **(A)**.

observed in the *indh* mutant, demonstrating the importance of *INDH* for plant growth and development.

INDH Is Required for Complex I Assembly

To investigate whether INDH plays a role in complex I assembly in plants, the levels and integrity of respiratory complexes were analyzed by blue-native polyacrylamide gel electrophoresis (BN-PAGE) and activity staining. Mitochondria were isolated from the wild-type, *indh* mutant, and complemented seedlings, and protein complexes were solubilized with dodecyl maltoside and separated by BN-PAGE. Gels were stained with Coomassie blue, or incubated with NADH and nitro blue tetrazolium to visualize the NADH dehydrogenase activity of complex I, which runs at the top of the gel because of its large ~1 MD size. Neither Coomassie blue–stained protein nor activity staining was detected at the expected position of complex I in the *indh*

mutant (Figure 5A; see Supplemental Figure 4 online), correlating with the absence of INDH protein (Figure 5B). By contrast, the assembly and activity of complex I was restored in the line overexpressing wild-type *INDH* cDNA in the *indh* knockout line (*indh* + *cINDH*). While complex V was intact in the *indh* mutant, a decrease in the levels of complex III could sometimes be observed (Figure 5C). The levels of the Fe-S binding protein aconitase and the Fe-S scaffold ISU1 were normal in *indh* seedlings (Figure 5B). The results indicate that, like in *Y. lipolytica* and in humans, depletion of INDH specifically affects complex I assembly and there is little or no effect on other respiratory complexes or mitochondrial Fe-S proteins.

Following recent progress in our knowledge of assembly intermediates of complex I (Meyer et al., 2011; Mimaki et al., 2012), we investigated the assembly of complex I in the *indh* mutant. Blots of BN-PAGE–separated membrane complexes were probed with antibodies against Nad6 or gamma carbonic anhydrases (CAs). Nad6 is a conserved integral membrane subunit, whereas CAs form a subdomain of the membrane arm of complex I that is unique to plants (Perales et al., 2004). The labeling patterns with either Nad6 or CAs antibodies showed a weak signal at 650 kD in the *indh* mutant that is absent from wild type. The relatively low intensity of the 650-kD signal compared with fully assembled complex I in the wild type, suggests that only a small amount of the assembly intermediate accumulates. Minor amounts of 450-kD and 400-kD intermediates were revealed upon longer exposure (Figure 5C). Based on analysis of *Arabidopsis* mutants in structural complex I subunits, the 650-, 450-, and 400-kD intermediates are thought to correspond to assembly modules of the membrane arm (Meyer et al., 2011).

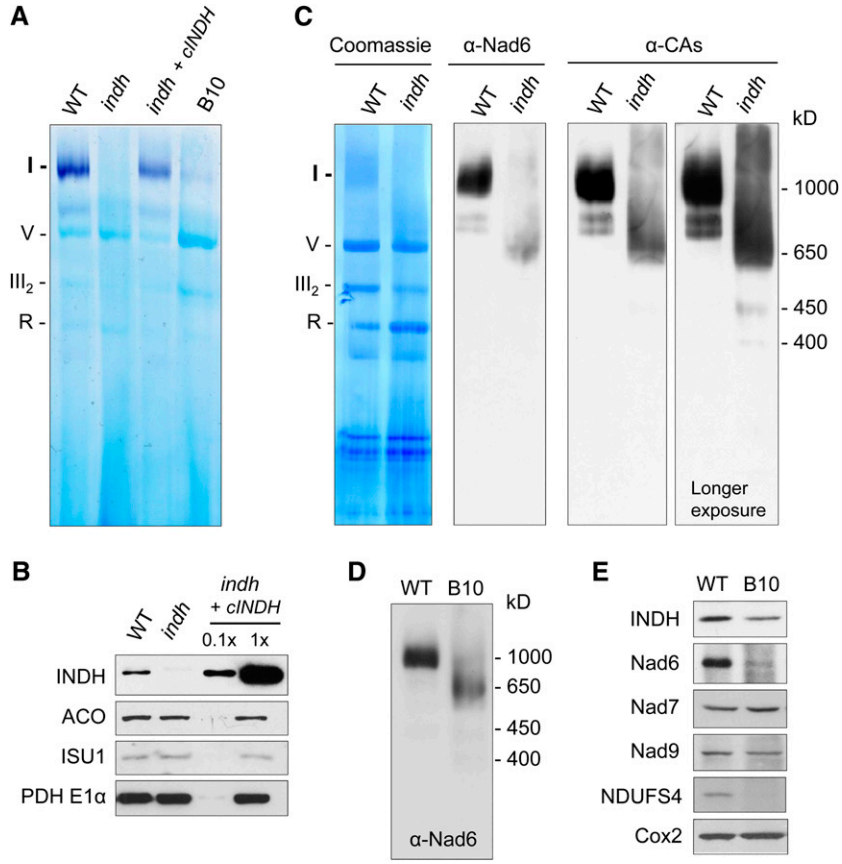

Figure 5. INDH Is Required for Complex I Assembly

(A) Complex I (I) is not assembled in the *indh* mutant. Mitochondria (50 μg protein) were isolated from the wild type (WT), the *indh* knockout mutant, the complemented *indh* mutant (*indh* + *cINDH*), and the B10 line (low INDH expression). Respiratory complexes were separated by BN-PAGE and stained with NADH and nitroblue tetrazolium for oxidoreductase activity of complex I (purple). Coomassie blue staining of other protein complexes is visible in lighter blue: complex V (F_1F_0 ATPase, V), the dimer of complex III (cytochrome bc_1 oxidoreductase, III_2), and contamination with Rubisco (R). The identity of the complexes was confirmed on the basis of the subunit pattern in the second dimension (see Supplemental Figure 4 online).

(B) Disruption of INDH does not affect aconitase (ACO) and ISU1 levels. Mitochondria (10 μg protein) were analyzed by immunoblotting for the indicated proteins. Antibodies against the E1α subunit of pyruvate dehydrogenase (PDH) were used as a loading control.

(C) and **(D)** Assembly intermediates of complex I in wild-type and *indh* mutants. Mitochondrial membranes were separated by BN-PAGE and blotted to polyvinylidene fluoride membrane. Protein complexes were stained with Coomassie blue [left panel in **(C)**], followed by immunolabeling with antibodies against Nad6 or carbonic anhydrases associated with complex I (α-CAs). B10 is a partially complemented *indh* line.

(E) Levels of complex I subunits and Cox2 in purified mitochondria as used in **(D)**.

We also investigated the presence of assembly intermediates and complex I subunits in a weaker allele of *indh*, named B10 (see below). The 650-kD assembly intermediate is also detected in this line (Figure 5D). Immunolabeling of the same mitochondrial preparations separated by SDS-PAGE showed that the levels of different complex I subunits varied (Figure 5E). The level of mitochondrially encoded Nad6 was strongly diminished and Nad7 was slightly increased, whereas Nad9 was decreased to ~50% in the mutant compared with the wild type. The nuclear-encoded NADH Dehydrogenase Ubiquinone Fe-S Protein 4 (NDUFS4) subunit was also strongly decreased. Although it is not possible to obtain a full overview of the protein levels of all individual subunits because of the limited availability of antibodies, the results indicate that some complex I subunits are present but not assembled (Nad7, Nad9), whereas others may be degraded or downregulated (Nad6, NDUFS4).

Reassembly of Complex I Is Significantly Delayed upon Expression of INDH Protein

One of the *35S:cINDH*-complemented *indh* homozygous lines, which we named B10, was delayed in early development, but growth was more vigorous than in *indh* after the initial 2 weeks, which was particularly noticeable in the absence of Suc (see Supplemental Figure 3 online). Immunoblot analysis on isolated mitochondria showed that INDH protein levels in the B10 line were below the detection level in germinating seedlings (stage 0.7, according to Boyes et al. [2001]). However, INDH levels increased gradually during vegetative development, reaching ~250% in mature rosette leaves (stage 3.90) (Figures 6 and 7). The low expression of *cINDH* in young seedlings correlated with poor resistance to hygromycin, suggesting that the T-DNA was inserted in a heterochromatin region that suppressed expression at early development. Backcrossing and genetic analysis of the B10 line showed that the observed phenotypes were linked to partial complementation of *indh* and were not attributable to disruption of another gene (see Supplemental Table 2B online).

We noticed that in the B10 line, the level of INDH protein correlated poorly with fully assembled complex I. For example, in the mitochondria preparation used for Figures 5D and 5E, INDH levels were 50% of the wild type, but no fully assembled complex I was detectable by immunoblot analysis. To quantify the relationship between INDH protein and complex I levels, data from different mitochondrial preparations were arranged by growth stage of the seedlings. This reduced variation between B10 seed batches, but also paired B10 and the wild type of the same growth stage. The level of fully assembled complex I was assessed from scans of formazan-stained BN-PAGE gels, and INDH expression was quantified from immunoblotting data, in both cases using ImageJ software. We found that reassembly of complex I lagged significantly behind de-repression of INDH (Figure 6). Complex I levels in the B10 line reached 100% only at growth stage 3.90, or mature rosettes, which is 2 weeks after growth stage 1.04 when INDH expression reached >100% of wild-type levels. The dynamics of complex I assembly in *Arabidopsis* was recently described for the first time (Li et al., 2013). Reassembly of complex I was apparent 20 min after reintroduction of the CA2 subunit in isolated mitochondria of a *ca2* mutant. Therefore, our data suggest that INDH may have an indirect role in complex I assembly.

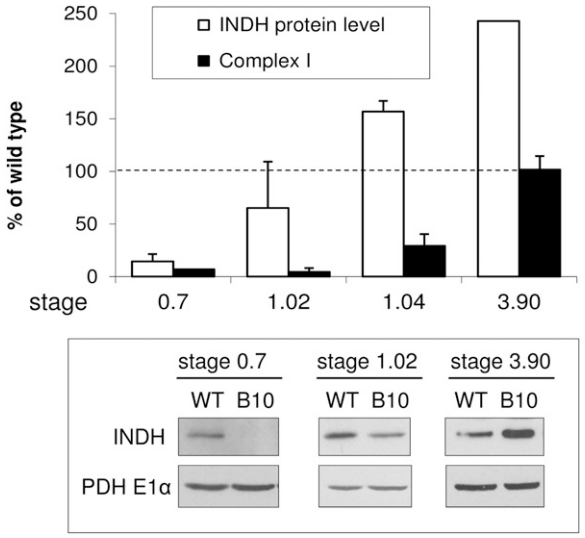

Figure 6. Restoration of Complex I Assembly Is Significantly Delayed after Gradually Increased INDH Expression in the *indh* Background.

Mitochondria were purified from wild-type (WT) and B10 mutant plants at growth stage 0.7 (hypocotyl and cotyledon emergence), stage 1.02 (green seedlings with two leaves >1 mm), stage 1.04 (four leaves >1 mm), and stage 3.90 (fully grown rosettes). The amount of fully assembled complex I was quantified from BN-PAGE gels, as well as INDH from immunostaining signals using ImageJ software. Representative immunostaining results are shown. Values are as a percentage of wild type at the same growth stage, ± SD (n = 2). Antibodies against pyruvate dehydrogenase (PDH) E1α were used as a loading control.

INDH Is Required for Mitochondrial Translation

The indirect correlation between INDH and complex I levels suggested that INDH is involved in mitochondrial gene expression. This idea was also hinted at by the unusual combination of phenotypes of *indh*/+ and *indh* mutants during the reproductive phase, which are more similar to those reported for mutants in mitochondrial translation than for complex I mutants (Table 1; see Discussion). To investigate whether INDH has a function in translation and how this would correlate with complex I assembly, we isolated mitochondria from different growth stages of the B10 line, followed by ^{35}S-Met labeling in organello. The earliest growth stage at which we managed to obtain mitochondria were germinating seeds from which the root was just emerging (growth stage 0.5). The total protein pattern of the organellar fraction was similar in B10 and the wild type (Figure 7A, left panel). However, very little radiolabel was incorporated in the INDH-depleted mitochondria compared with the wild type, indicating that the rate of translation is strongly decreased. We also isolated mitochondria at growth stages 0.7 and 1.02 with 20% and 58% of wild-type INDH protein levels, respectively (Figure 7B). Both the translation rate and protein pattern changed markedly during seedling germination and greening, concomitant with increased mitochondrial biogenesis and

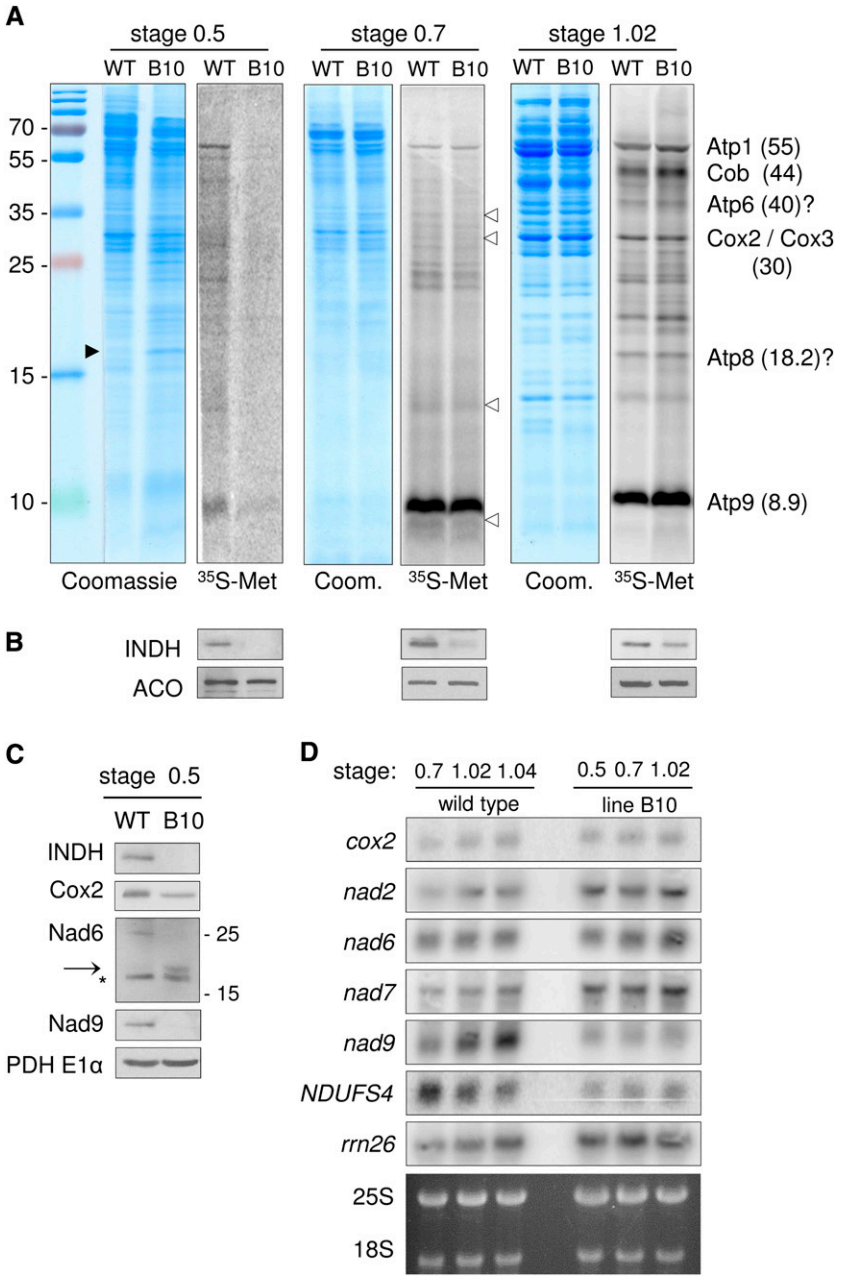

Figure 7. INDH Plays a Role in Mitochondrial Protein Translation.

(A) ^{35}S-Met labeling of purified mitochondria from wild-type (WT) and INDH-depleted seedlings (B10) at different growth stages. Stage 0.5 is root emergence; see Figure 6 for the other stages. The seedlings were grown under sterile conditions to avoid problems with bacterial contamination in the translation assay. After exposure to reveal the radioactivity signal, total protein was stained with Coomassie blue. The arrowheads point to noticeable differences in band intensities between WT and B10. The assignment of proteins on the right is based on other reports and molecular mass, in parentheses. A question mark indicates that the assignment is tentative. Atp, subunit of ATP synthase (complex V); Cob, cytochrome *b*; Cox, subunit of cytochrome *c* oxidase.

(B) Levels of INDH and aconitase (ACO) in the mitochondrial fractions used in **(A)**, visualized by immunoblotting.

(C) Protein levels of mitochondrial-encoded Cox2, Nad6, and Nad9 in stage 0.5 mitochondria of the wild type and the B10 line. The E1α subunit of pyruvate dehydrogenase (PDH) was labeled as control. The arrow indicates a putative breakdown product of Nad6. The asterisk indicates a nonspecific immunoreactive protein.

(D) mRNA levels of selected mitochondrial transcripts (as indicated) and the nuclear-encoded *NDUFS4* at different developmental stages. The lower panel shows the ethidium-bromide stained 25S and 18S ribosomal subunits in the gel before blotting and serves as loading control.

[See online article for color version of this figure.]

Table 1. Comparison of *indh*/+ with Selected Mutants in Complex I and Mitochondrial Biogenesis

Mutant	Protein	Segregation[a]	Transmission (%)		Pollen (% dead)	Reference
			Female	Male		
indh (GK_956A05)	INDH	0: 1: 1 (−Suc) 0.7: 1: 1 (+Suc)	96	89	40–50	This study
emb1467, 75kD (N16195)[b]	75-kD subunit of complex I	0: 2: 1 (−Suc) 0.02: 2: 1 (+Suc)	ND	ND	Normal	This study
nfd1 (nuclear fusion deficient)*	Mit RPL21	0: 0.7:1	20.8	22	42	Portereiko et al. (2006)
nfd3	Mit RPS11	0: 0.9:1	25.9	3	ND	Portereiko et al. (2006)
mrpl11	Mit RPL11	1: 2: 1[c]	-	-	-	Pesaresi et al. (2006)
prors (ova6)	Prolyl-tRNA synthetase	0: 0.7: 1	ND	ND	40	Berg et al. (2005); this study
prors1-3		0: 0.9:1	27	89	ND	Pesaresi et al. (2006)
ilers (ova2)	Isoleucyl-tRNA synthetase	0: 1.1: 1	70	60	33	Berg et al. (2005); this study
gfa2 (nfd)	Mjd1-like (chaperone)	0: 1: 1	99	86	ND	Christensen et al. (2002)

ND, not determined.
[a]Segregation is given in the following order, homozygous mutant: heterozygous: wild type.
[b]N16195 has a T-DNA insertion in exon 5 in gene *AT5G37510* and was previously found in a screen for embryo-lethal mutants (www.seedgenes.org). *AT5G37510* encodes the 75-kD subunit of complex I, which binds three Fe-S clusters. A very low frequency (1 in 50) of homozygous mutants was obtained, which were viable and produced low numbers of seed.
[c]RPL11 is not an essential ribosomal subunit, but is added for comparison.

changes in metabolic functions (Law et al., 2012). Although the rate of translation was restored correlating with expression of INDH, minor differences in de novo synthesis of specific proteins could be seen in B10 mitochondria with 20% INDH (indicated by white arrowheads in Figure 7A; see also the protein profile plot in Supplemental Figure 5 online).

Unfortunately, the mitochondrial in organello labeling pattern is poorly characterized in plants compared with humans. The most prominent upper and lower signals are thought to be Atp1 and Atp9, two highly abundant mitochondrial proteins of the ATP synthase complex (Giegé et al., 2005); however, the identity of other translation products is uncertain. To investigate the steady state levels of mitochondrially encoded proteins, in particular at stage 0.5, mitochondrial fractions were labeled with antibodies against cytochrome *c* oxidase subunit2 (Cox2), Nad6, and Nad9 (Figure 7C). Cox2 levels were 50% less in the B10 mitochondria, while Nad6 and Nad9 levels fell below the detection limit. A prominent lower-mass protein of ~18 kD with affinity to the Nad6 antibodies was specifically detected in B10 mitochondria. This may be a breakdown product of Nad6. Note that at stage 1.02 of development when INDH expression was ~50%, Cox2 protein levels were restored to normal and Nad9 levels were 50% compared with the wild type (Figure 5E). Nad6 protein levels were still severely depleted at this stage.

Last, we investigated whether the decrease in specific mitochondrial proteins was a result of lower transcript levels rather than a posttranscriptional defect. Total RNA was isolated from wild-type and B10 seedlings at different developmental stages and probed for selected mitochondrial and nuclear transcripts using RNA gel blotting (Figure 7D). mRNA levels of *cox2*, *nad2*, *nad6*, and *nad7* and the rRNA *rrn26* were normal or increased; however, *nad9* and the nuclear-encoded *NDUFS4* transcripts were decreased in the B10 line.

These data suggest that INDH has a role in the translation of mitochondrial proteins, with a differential effect on specific polypeptides, which could cause the delay in complex I assembly upon de-repression of INDH.

DISCUSSION

The evolutionary drive for both increased size of OXPHOS complexes and retention of selected genes in the mitochondrial genome comes with a great cost. Many extra proteins are required to orchestrate mitochondrial gene expression, to import nuclear-encoded proteins, and to assemble the numerous subunits and prosthetic groups in an orderly fashion. In addition, the complex assembly process is prone to errors, which can cause loss of fitness, including debilitating diseases. The Ind1 protein was previously identified as an assembly factor of complex I in the yeast *Y. lipolytica* (Bych et al., 2008b) and subsequently in human cells (Sheftel et al., 2009) and was linked to pathogenic complex I deficiencies (Calvo et al., 2010; Tenisch et al., 2012; Kevelam et al., 2013). Here, we show that INDH, the homolog of Ind1 in the model plant *Arabidopsis*, is also specifically required for complex I assembly. However, we found that its function(s) may be more compound than initially proposed.

INDH can be defined as an assembly factor of complex I in *Arabidopsis* in the sense that it is not associated with mature complex I (Figure 1C) and mutation resulted in the specific loss of complex I (Figure 5). In addition, slow vegetative growth is generally observed in *Arabidopsis* complex I mutants (see Supplemental Figure 3 online). Based on its homology to P-loop NTPases involved in Fe-S cluster assembly (Roy et al., 2003; Lezhneva et al., 2004; Netz et al., 2007; Schwenkert et al., 2010), and binding of a transferable Fe-S cluster, we previously proposed that this protein functions as a Fe-S scaffold specific for complex I (Bych et al., 2008b). Indeed, the assembly intermediates

of complex I found in *Arabidopsis* mitochondria depleted of INDH would be consistent with this idea (Figures 5C and 5D). The accumulation of a 650-kD subcomplex is similar to that in *Arabidopsis* mutants lacking the peripheral arm subunits NDUFS4 or 39-kD (NDUFA9) (Meyer et al., 2011). The 650-kD subcomplex in the *ndufs4* mutant was shown to lack the N-module that contains Fe-S cluster binding subunits. However, the relatively small amounts of 650-kD intermediate in the *indh* knockout mutant (Figure 5A) suggest that there may be an additional defect in the assembly of the membrane arm, which does not contain Fe-S proteins.

Interestingly, our in-depth characterization of *Arabidopsis indh* mutant alleles indicates that INDH has a function in mitochondrial translation. One explanation is that the lack of complex I, and consequently lower ATP levels, leads to impaired translation; however, we think this is not the case. First, the ^{35}S-Met incorporation studies were done using isolated organelles with added ATP and GTP. Second, at growth stage 1.02, complex I levels were only 30%, whereas in organello translation rates were restored to normal (Figures 6 and 7A). Third, recent studies in human cells showed that depletion of early complex I assembly factors resulted in increased proteolysis of the ND1 subunit, rather than a block in its translation (Zurita Rendón and Shoubridge, 2012). The long delay in complex I restoration upon de-repression of INDH (Figure 6) is also indicative of a translation defect. In human cell lines, reassembly of complex I upon expression of a missing structural subunit took less than 24 h (Dieteren et al., 2012), whereas reassembly after transient inhibition of mitochondrial translation took 2 to 4 d (Ugalde et al., 2004).

Further support for the idea that INDH may play a role in mitochondrial translation comes from the unusual combination of phenotypes in heterozygous *indh*/+ plants. Aberrant segregation ratios, and abortion of both ovules and pollen but near-normal transmission of the mutant allele (Figure 3) have also been observed in plants that are heterozygous for insertion alleles of genes encoding essential mitochondrial ribosomal subunits or amino acid tRNA synthetases (Table 1). By contrast, mutants that completely lack complex I (de Longevialle et al., 2007; Meyer et al., 2009) or lack the 75-kD Fe-S binding subunit (Table 1) do not show gametophytic defects in the heterozygotes, and segregate like essential genes. How could loss of one functional allele required for mitochondrial translation cause random abortion of gametophytes? First, reproductive development in plants is known to reveal even minor impairments in OXPHOS, such as in a class of mitochondrial mutants known as cytoplasmic male sterility mutants. Second, nuclear gene expression shuts down during meiosis; therefore, the early stages of gametogenesis rely on sufficient reserves in metabolites but also amino-acylated tRNAs. Apparently, the amount of amino acid tRNA in the mitochondria is only just enough to survive the shutdown period, since haploinsufficiency of a specific amino acid tRNA synthetase can lead to random death of female and male gametophytes after meiosis (Berg et al., 2005). Something similar might occur in the *indh*/+ mutant. Analysis of the *indh* allele in the *quartet1-2* background showed that death of a particular pollen daughter cell is independent of meiotic segregation of the *indh* allele or positional cues in the pollen sack (Figure 3F; see Supplemental Figure 6 online). Instead, it is likely that a daughter cell dies because of uneven segregation of a mitochondrial population with variable translation capacities. It would be interesting to investigate whether cell death is the consequence of low ATP levels or another aspect of mitochondrial function. We have analyzed ATP levels in illuminated rosette leaves, which was not significantly lower in soil-grown *indh* compared with the wild type despite severe growth retardation in *indh* (see Supplemental Figure 7 online). Moreover, in seedlings grown on a medium containing Suc, ATP levels were in fact higher in the *indh* mutant, indicating that mechanisms have been induced to compensate for lack of complex I.

The *Arabidopsis* tRNA synthetase mutants could perhaps be thought of as the equivalent to human mitochondrial tRNA (mt-tRNA) mutations, which have thus far not been found in plants. Interestingly, mutations in several human mt-tRNAs have been reported to cause isolated complex I deficiency, with no obvious effect on other respiratory complexes. These include the mt-tRNA for Pro, Trp, Lys, Leu (UUR), and Ser (AGY) (Shoffner et al., 1990; Arenas et al., 1999; Blakely et al., 2009; Da Pozzo et al., 2009; Calvo et al., 2010; Swalwell et al., 2011). Although little is known about mitochondrial translation in plants, a recent study (Kwasniak et al., 2013) described how silencing of *RPS10*, a nuclear-encoded subunit of the small ribosomal subunit in mitochondria, resulted in an altered pattern of in organello–translated peptides. The protein level and activity of complex I was the most affected of the respiratory complexes. These data indicate that a generic defect in mitochondrial translation can have a differential effect on individual peptides, and that complex I is most vulnerable because of its large number of mitochondrially encoded subunits.

In conclusion, our results indicate that INDH plays an indirect role in complex I assembly, through the biogenesis of mitochondrially encoded proteins. At the moment, our data do not fully exclude the previously proposed role in inserting Fe-S clusters, but this is less likely given the time-dependent difference in INDH levels and fully assembled complex I (Figure 6). Although the role of INDH in translation could be specific for *Arabidopsis*, it may be worth investigating for *Y. lipolytica* and human. It was previously noted that *ind1*Δ *Yarrowia* could not go through meiosis, which is perhaps a result of gametogenesis problems (Bych et al., 2008b); in addition, other respiratory complexes in NUBPL-depleted cells are also mildly affected (Calvo et al., 2010). Ultimately, any further knowledge on the precise role of IND1 and its homologs will help to elucidate why this conserved protein is important for complex I assembly and why certain aspects of mitochondrial biogenesis are critical for both male and female gametogenesis.

METHODS

Plant Material and Growth

The *Arabidopsis thaliana* line GK_956A05 was obtained from the Gabi-Kat collection (Kleinboelting et al., 2012). Insertion of a single T-DNA in the *INDH* gene (*AT4G19540*) was confirmed by PCR, sequencing of the left border, and the segregation of sulfadiazine resistance. The heterozygous *ova2*/+, *ova6*/+, and *emb1467*/+ lines were obtained from the Nottingham *Arabidopsis* Stock Centre (stock IDs SALK_088424, SALK_045080, and

N16195, respectively). The *quartet1-2* mutant was provided by Ian R. Henderson (University of Cambridge). The *ndufs4* and *rug3-1* mutants were previously described (Meyer et al., 2009; Kühn et al., 2011). Primers used to confirm the genotype of the lines by standard PCR procedures are listed in Supplemental Table 3 online. Plants were grown on agar plates containing one-half-strength Murashige and Skoog salts, with 1% (w/v) Suc when indicated, and antibiotics when required for selection. Seedlings for mitochondria preparations were grown in hydroponic culture (Sweetlove et al., 2007). All plants were grown under a 16/8 h light/dark cycle with a photon flux density of 100–150 μmol m^2 s^{-1} at 20°C and 65% relative humidity. Because of the developmental delay in the B10 line, we compared plant material at the same growth stages as defined by Boyes et al. (2001).

cINDH Expression

A cDNA corresponding to full-length *INDH* (c*INDH*) was cloned in fusion with *GFP* in the pOL-GFP-S65C vector using the *Spe*I and *Sal*I restriction sites (Peeters et al., 2000), and expressed transiently using particle bombardment of *Arabidopsis* leaves. For complementation of the mutant allele, *cINDH* was cloned behind the 35S CaMV promoter and translational enhancer in the pBIN vector, or behind the *UBIQUITIN11* promoter (*UQ11*) in the pART27 vector (Gleave, 1992). The restriction sites *Nco*I and *Xba*I were used to clone *cINDH* behind the 35S promoter, and *Asc*I and *Pac*I to transfer *35S:cINDH* to pBIN. The restriction sites *Xho*I and *Bam*HI were used to clone *cINDH* behind the *UQ11* promoter, and *Not*I to transfer UQ11:cINDH to pART27. The pBIN and pART27 vectors carried hygromycin B or kanamycin resistance, respectively, as a selectable marker. Plants were transformed using *Agrobacterium tumefaciens*–mediated insertion of the T-DNA. Primers for the cloning and for PCR detection are listed in Supplemental Table 3 online.

Microscopy

Immature ovules were imaged with differential interference contrast microscopy after tissue clearing with Hoyer's solution (Ruzin, 1999). Flowers were embedded with polyethylene glycol, sectioned, and stained with toluidine blue. Pollen was stained with Alexander's stain (Alexander, 1969). Stained sections and pollen were analyzed using conventional light microscopy. Green fluorescent protein and chlorophyll autofluorescence were visualized by confocal microscopy (Leica DM RXA).

Purification of Mitochondria and Other Cell Fractions

Plant mitochondria were purified from germinating seeds using differential centrifugation. When using hydroponic seedlings or rosette leaves as source material, the mitochondria were further purified using a Percoll and polyvinylpyrrolidine-40 gradient (Sweetlove et al., 2007). *Yarrowia lipolytica* mitochondria were purified by differential centrifugation (Daum et al., 1982). Chloroplasts were isolated from rosette leaves. Total cell extract was prepared from leaves by grinding tissue with 2 vol of buffer (50 mM Tris-HCl 8.0, 0.1% [w/v] sodium dodecyl maltoside, 1 mM ETDA, 1 mM phenylmethylsulfonyl fluoride, 1 mM dithiothreitol) and centrifuging for 10 min at 16,000*g* to remove debris. The protein concentration was determined using the Bradford method (Bio-Rad Protein Assay).

Protein Blot Analysis

Total cell extract or purified organelles were mixed with Laemmli buffer and separated on standard SDS-PAGE gels. Proteins were transferred to nitrocellulose (Schleicher & Schuell BA 83), and labeled with antibodies. Immunolabeling was detected using secondary horseradish peroxidase–conjugated antibodies and chemiluminescence.

Rabbit polyclonal antibodies were raised against purified His-tagged INDH protein and were affinity purified before use. The antibodies against aconitase and NBP35 were previously described (Bych et al., 2008a; Bernard et al., 2009). Mouse monoclonal antibodies against the E1α subunit of pyruvate dehydrogenase and porin were from GTMA. Details for the following antibodies are as published: Nad7 and Nad9 (Lamattina et al., 1993), ISU1 and PetC (Bych et al., 2008a), CA2 (Perales et al., 2004), and Nad6 (Koprivova et al., 2010).

Blue-Native PAGE and Activity Staining

Blue-native PAGE was performed as described in Wittig et al. (2006) for activity staining, and as described in Meyer et al. (2011) for immunolabeling. Gels were incubated with 0.2 mM NADH and 0.1% (w/v) nitroblue tetrazolium in 0.1 M Tris-HCl 7.4 for NADH dehydrogenase activities. For immunolabeling, gels were blotted onto polyvinylidene difluoride.

In Organello Translation

Purified mitochondria from plants grown under sterile conditions were labeled with ^{35}S-Met as previously described with minor modifications (Giegé et al., 2005). In brief, mitochondria (100 μg protein) were pelleted and resuspended in 0.1 mL 0.3 M mannitol, 50 mM HEPES-KOH pH 7.4, 60 mM KCl, 10 mM $MgCl_2$, 5 mM KH_2PO_4, 0.1% (w/v) BSA, 10 mM Na-malate, 10 mM Na-pyruvate, 2 mM GTP, 4 mM ADP, 4 mM ATP, and 2 mM dithiothreitol. Unlabeled amino acid mix without Met (2.5 μL 1 mM each, Promega) was added and the mixture was preincubated for 15 min at 23°C attached to a rotating wheel (15 rpm). After addition of ^{35}S-Met (30 μCi of EasyTag L-[^{35}S]-Methionine; PerkinElmer), the mitochondria were incubated for 1 h. Label incorporation was stopped by adding 0.5 mL 0.3 M mannitol, 50 mM HEPES-KOH pH 7.4, 10 mM Met. Mitochondria were pelleted by centrifugation and resuspended in 1× Laemmli buffer. The samples were separated on 15% SDS-PAGE gels, dried and exposed to a phosphor-imaging plate. Exposure ranged from 1 week (Percoll-purified mitochondria from 10-d-old seedlings) to 12 weeks (mitochondria from germinating seeds). After exposure, the gel was rehydrated and stained with Coomassie Brilliant Blue R 250 (InstantBlue; Expedeon).

RNA Isolation and RNA Gel Blot Analysis

Total cellular RNA was isolated from 30- to 50-mg seedlings using an RNeasy Plant Mini (Qiagen) kit according to the manufacturer's instructions. For RNA gel blot analysis 2.5 to 5 μg of RNA was separated on 1.2% (w/v) agarose gels using formaldehyde as denaturing agent. Gel electrophoresis, blotting, and hybridization were done as previously described (Sambrook and Russel, 2001). Nucleic acids were blotted onto Hybond-N+ membrane (GE Healthcare) and hybridized with ^{32}P radiolabeled oligonucleotides (*cox2*, *rrn23*) or PCR-generated probes (*nad2*, *nad6*, *nad7*, *nad9*). Oligonucleotides used are listed in Supplemental Table 3 online.

Statistical Analysis

For genetic analysis, the chi-squared test for goodness of fit was applied. Numerical values are the average of independent experimental replicates, with *n* indicated in the figure legends. Error bars represent the standard deviation.

Accession Numbers

Sequence data from this article can be found in the *Arabidopsis* Genome Initiative or GenBank/EMBL data libraries under accession number *INDH* (*AT4G19540*) and in Table 1. The accession numbers for other genes/proteins studied in this work are as follows: 75-kD subunit, also named NUAM (AT5G37510), aconitase (AT4G35830, AT4G26970, AT2G05710), gamma CA2 (AT1G47260), Cox2 (ATMG00160), *ILERS* (*AT5G49030*),

ISU1 (AT4G22220), Nad2 (ATMG00285), Nad6 (ATMG00270), Nad7 (ATMG00510), Nad9 (ATMG00070), NBP35 (AT5G50960), NDUFS4 (AT5G67590), PDH E1α (AT1G59900, AT1G24180), PetC (AT4G03280), Porin (VDAC, 5 paralogs: AT3G01280, AT5G67500, AT5G15090, AT5G57490, AT5G15090); *PRORS* (*AT5G52520*), *RUG3* (*AT5G60870*), *rrn26* (*ATMG00020*), and *UBIQUITIN11* (*AT4G05050*).

Supplemental Data

The following materials are available in the online version of this article.

Supplemental Figure 1. Amino Acid Alignment of INDH and Homologs.

Supplemental Figure 2. Distribution of Tetrad Configurations in *indh*/+ Heterozygotes.

Supplemental Figure 3. Growth of *indh* Compared with Other Complex I Mutants.

Supplemental Figure 4. Identification of Respiratory Complexes in BN-PAGE.

Supplemental Figure 5. Plot Profiles of ^{35}S-Met Labeling in Organello.

Supplemental Figure 6. The Locule of an *indh*/+ Plant Contains Clusters of Dead Pollen.

Supplemental Figure 7. ATP Levels in Leaf Tissue and Seedlings.

Supplemental Table 1. Segregation Analysis of the T-DNA Insertion in the *INDH* Gene.

Supplemental Table 2. Genetic Analysis of *indh* (GK_956A05) and B10 Mutant Lines.

Supplemental Table 3. Primers Used in This Study.

ACKNOWLEDGMENTS

We thank Roland Lill for antibodies against INDH, ACO1, Leu1, and Nfs1; Ian Small and Cathie Colas des Francs-Small for antibodies against Nad6; Jean-Michel Grienenberger for antibodies against Nad7 and Nad9; Eduardo Zabaleta for antibodies against CAs; Stephane Lobréaux for antibodies against ISU1; John C Gray for antibodies against PetC; Jim Haseloff for the pOL-GFP vector; Ben Hunter and Ian Furner for the UBQ11 promoter; Liz Alvey for help with confocal microscopy; and Luke Browning for technical assistance. This work was funded by the Deutscher Akademischer Austausch Dienst (P.S.), Wellcome Trust (WT089291MA, M.M.W. and J.F.), Danish Research Agency, Carlsberg Foundation (K.B.), and the Royal Society (J.B.).

AUTHOR CONTRIBUTIONS

M.M.W., K.B., and E.H.M. designed and performed research and analyzed data. P.S. performed research and analyzed data. J.M.F. performed research. J.B. designed and performed research, analyzed data, and wrote the article, with most valuable feedback from M.M.W. and E.H.M.

Received August 11, 2013; revised September 29, 2013; accepted October 15, 2013; published October 31, 2013.

REFERENCES

Alexander, M.P. (1969). Differential staining of aborted and nonaborted pollen. Stain Technol. **44:** 117–122.

Arenas, J., Campos, Y., Bornstein, B., Ribacoba, R., Martín, M.A., Rubio, J.C., Santorelli, F.M., Zeviani, M., DiMauro, S., and Garesse, R. (1999). A double mutation (A8296G and G8363A) in the mitochondrial DNA tRNA (Lys) gene associated with myoclonus epilepsy with ragged-red fibers. Neurology **52:** 377–382.

Balk, J., and Leaver, C.J. (2001). The PET1-CMS mitochondrial mutation in sunflower is associated with premature programmed cell death and cytochrome *c* release. Plant Cell **13:** 1803–1818.

Berg, M., Rogers, R., Muralla, R., and Meinke, D. (2005). Requirement of aminoacyl-tRNA synthetases for gametogenesis and embryo development in *Arabidopsis*. Plant J. **44:** 866–878.

Bernard, D.G., Cheng, Y., Zhao, Y., and Balk, J. (2009). An allelic mutant series of ATM3 reveals its key role in the biogenesis of cytosolic iron-sulfur proteins in Arabidopsis. Plant Physiol. **151:** 590–602.

Blakely, E.L., Trip, S.A., Swalwell, H., He, L., Wren, D.R., Rich, P., Turnbull, D.M., Omer, S.E., and Taylor, R.W. (2009). A new mitochondrial transfer RNA^{Pro} gene mutation associated with myoclonic epilepsy with ragged-red fibers and other neurological features. Arch. Neurol. **66:** 399–402.

Boyes, D.C., Zayed, A.M., Ascenzi, R., McCaskill, A.J., Hoffman, N. E., Davis, K.R., and Görlach, J. (2001). Growth stage-based phenotypic analysis of *Arabidopsis*: A model for high throughput functional genomics in plants. Plant Cell **13:** 1499–1510.

Brandt, U. (2006). Energy converting NADH:quinone oxidoreductase (complex I). Annu. Rev. Biochem. **75:** 69–92.

Bych, K., Netz, D.J., Vigani, G., Bill, E., Lill, R., Pierik, A.J., and Balk, J. (2008a). The essential cytosolic iron-sulfur protein Nbp35 acts without Cfd1 partner in the green lineage. J. Biol. Chem. **283:** 35797–35804.

Bych, K., Kerscher, S., Netz, D.J., Pierik, A.J., Zwicker, K., Huynen, M.A., Lill, R., Brandt, U., and Balk, J. (2008b). The iron-sulphur protein Ind1 is required for effective complex I assembly. EMBO J. **27:** 1736–1746.

Calvo, S.E., et al. (2010). High-throughput, pooled sequencing identifies mutations in *NUBPL* and *FOXRED1* in human complex I deficiency. Nat. Genet. **42:** 851–858.

Christensen, C.A., Gorsich, S.W., Brown, R.H., Jones, L.G., Brown, J., Shaw, J.M., and Drews, G.N. (2002). Mitochondrial GFA2 is required for synergid cell death in *Arabidopsis*. Plant Cell **14:** 2215–2232.

Colas de Francs-Small, C., and Small, I. (August 29, 2013). Surrogate mutants for studying mitochondrially encoded functions. Biochimie (online), doi10.1016/j.biochi.2013.08.019.

Da Pozzo, P., Cardaioli, E., Malfatti, E., Gallus, G.N., Malandrini, A., Gaudiano, C., Berti, G., Invernizzi, F., Zeviani, M., and Federico, A. (2009). A novel mutation in the mitochondrial tRNA(Pro) gene associated with late-onset ataxia, retinitis pigmentosa, deafness, leukoencephalopathy and complex I deficiency. Eur. J. Hum. Genet. **17:** 1092–1096.

Daum, G., Böhni, P.C., and Schatz, G. (1982). Import of proteins into mitochondria. Cytochrome b_2 and cytochrome *c* peroxidase are located in the intermembrane space of yeast mitochondria. J. Biol. Chem. **257:** 13028–13033.

de Longevialle, A.F., Meyer, E.H., Andrés, C., Taylor, N.L., Lurin, C., Millar, A.H., and Small, I.D. (2007). The pentatricopeptide repeat gene *OTP43* is required for trans-splicing of the mitochondrial *nad1* Intron 1 in *Arabidopsis thaliana.* Plant Cell **19:** 3256–3265.

Dieteren, C.E.J., Koopman, W.J.H., Swarts, H.G., Peters, J.G.P., Maczuga, P., van Gemst, J.J., Masereeuw, R., Smeitink, J.A., Nijtmans, L.G., and Willems, P.H. (2012). Subunit-specific incorporation efficiency and kinetics in mitochondrial complex I homeostasis. J. Biol. Chem. **287:** 41851–41860.

Efremov, R.G., and Sazanov, L.A. (2011). Respiratory complex I: 'Steam engine' of the cell? Curr. Opin. Struct. Biol. **21:** 532–540.

Francis, K.E., Lam, S.Y., and Copenhaver, G.P. (2006). Separation of *Arabidopsis* pollen tetrads is regulated by QUARTET1, a pectin methylesterase gene. Plant Physiol. **142:** 1004–1013.

Gabaldón, T., Rainey, D., and Huynen, M.A. (2005). Tracing the evolution of a large protein complex in the eukaryotes, NADH: ubiquinone oxidoreductase (Complex I). J. Mol. Biol. **348:** 857–870.

Giegé, P., Sweetlove, L.J., Cognat, V., and Leaver, C.J. (2005). Coordination of nuclear and mitochondrial genome expression during mitochondrial biogenesis in *Arabidopsis.* Plant Cell **17:** 1497–1512.

Gleave, A.P. (1992). A versatile binary vector system with a T-DNA organisational structure conducive to efficient integration of cloned DNA into the plant genome. Plant Mol. Biol. **20:** 1203–1207.

Hoefs, S.J., Rodenburg, R.J., Smeitink, J.A., and van den Heuvel, L.P. (2012). Molecular base of biochemical complex I deficiency. Mitochondrion **12:** 520–532.

Kevelam, , et al. (2013). *NUBPL* mutations in patients with complex I deficiency and a distinct MRI pattern. Neurology **80:** 1577–1583.

Kleinboelting, N., Huep, G., Kloetgen, A., Viehoever, P., and Weisshaar, B. (2012). GABI-Kat SimpleSearch: New features of the *Arabidopsis* thaliana T-DNA mutant database. Nucleic Acids Res. **40** (Database issue)**:** D1211–D1215.

Klodmann, J., Senkler, M., Rode, C., and Braun, H.P. (2011). Defining the protein complex proteome of plant mitochondria. Plant Physiol. **157:** 587–598.

Koprivova, A., des Francs-Small, C.C., Calder, G., Mugford, S.T., Tanz, S., Lee, B.R., Zechmann, B., Small, I., and Kopriva, S. (2010). Identification of a pentatricopeptide repeat protein implicated in splicing of intron 1 of mitochondrial *nad7* transcripts. J. Biol. Chem. **285:** 32192–32199.

Kühn, K., Carrie, C., Giraud, E., Wang, Y., Meyer, E.H., Narsai, R., des Francs-Small, C.C., Zhang, B., Murcha, M.W., and Whelan, J. (2011). The RCC1 family protein RUG3 is required for splicing of *nad2* and complex I biogenesis in mitochondria of *Arabidopsis thaliana.* Plant J. **67:** 1067–1080.

Kwasniak, M., Majewski, P., Skibior, R., Adamowicz, A., Czarna, M., Sliwinska, E., and Janska, H. (2013). Silencing of the nuclear RPS10 gene encoding mitochondrial ribosomal protein alters translation in *Arabidopsis* mitochondria. Plant Cell **25:** 1855–1867.

Lamattina, L., Gonzalez, D., Gualberto, J., and Grienenberger, J.M. (1993). Higher plant mitochondria encode an homologue of the nuclear-encoded 30-kDa subunit of bovine mitochondrial complex I. Eur. J. Biochem. **217:** 831–838.

Law, S.R., Narsai, R., Taylor, N.L., Delannoy, E., Carrie, C., Giraud, E., Millar, A.H., Small, I., and Whelan, J. (2012). Nucleotide and RNA metabolism prime translational initiation in the earliest events of mitochondrial biogenesis during Arabidopsis germination. Plant Physiol. **158:** 1610–1627.

Lezhneva, L., Amann, K., and Meurer, J. (2004). The universally conserved HCF101 protein is involved in assembly of [4Fe-4S]-cluster-containing complexes in *Arabidopsis thaliana* chloroplasts. Plant J. **37:** 174–185.

Li, L., Nelson, C.J., Carrie, C., Gawryluk, R.M., Solheim, C., Gray, M.W., Whelan, J., and Millar, A.H. (2013). Subcomplexes of ancestral respiratory complex I subunits rapidly turn over in vivo as productive assembly intermediates in *Arabidopsis*. J. Biol. Chem. **288:** 5707–5717.

Lill, R. (2009). Function and biogenesis of iron-sulphur proteins. Nature **460:** 831–838.

Meyer, E.H., Solheim, C., Tanz, S.K., Bonnard, G., and Millar, A.H. (2011). Insights into the composition and assembly of the membrane arm of plant complex I through analysis of subcomplexes in *Arabidopsis* mutant lines. J. Biol. Chem. **286:** 26081–26092.

Meyer, E.H., Tomaz, T., Carroll, A.J., Estavillo, G., Delannoy, E., Tanz, S.K., Small, I.D., Pogson, B.J., and Millar, A.H. (2009). Remodeled respiration in *ndufs4* with low phosphorylation efficiency suppresses Arabidopsis germination and growth and alters control of metabolism at night. Plant Physiol. **151:** 603–619.

Mimaki, M., Wang, X., McKenzie, M., Thorburn, D.R., and Ryan, M. T. (2012). Understanding mitochondrial complex I assembly in health and disease. Biochim. Biophys. Acta **1817:** 851–862.

Netz, D.J., Pierik, A.J., Stümpfig, M., Mühlenhoff, U., and Lill, R. (2007). The Cfd1-Nbp35 complex acts as a scaffold for iron-sulfur protein assembly in the yeast cytosol. Nat. Chem. Biol. **3:** 278–286.

Pagliarini, D.J., et al. (2008). A mitochondrial protein compendium elucidates complex I disease biology. Cell **134:** 112–123.

Peeters, N.M., Chapron, A., Giritch, A., Grandjean, O., Lancelin, D., Lhomme, T., Vivrel, A., and Small, I. (2000). Duplication and quadruplication of *Arabidopsis thaliana* cysteinyl- and asparaginyl-tRNA synthetase genes of organellar origin. J. Mol. Evol. **50:** 413–423.

Perales, M., Parisi, G., Fornasari, M.S., Colaneri, A., Villarreal, F., González-Schain, N., Echave, J., Gómez-Casati, D., Braun, H.P., Araya, A., and Zabaleta, E. (2004). Gamma carbonic anhydrase like complex interact with plant mitochondrial complex I. Plant Mol. Biol. **56:** 947–957.

Pesaresi, P., Masiero, S., Eubel, H., Braun, H.P., Bhushan, S., Glaser, E., Salamini, F., and Leister, D. (2006). Nuclear photosynthetic gene expression is synergistically modulated by rates of protein synthesis in chloroplasts and mitochondria. Plant Cell **18:** 970–991.

Portereiko, M.F., Sandaklie-Nikolova, L., Lloyd, A., Dever, C.A., Otsuga, D., and Drews, G.N. (2006). NUCLEAR FUSION DEFECTIVE1 encodes the Arabidopsis RPL21M protein and is required for karyogamy during female gametophyte development and fertilization. Plant Physiol. **141:** 957–965.

Roy, A., Solodovnikova, N., Nicholson, T., Antholine, W., and Walden, W.E. (2003). A novel eukaryotic factor for cytosolic Fe-S cluster assembly. EMBO J. **22:** 4826–4835.

Ruzin, S.E. (1999). Plant Microtechnique and Microscopy. (Oxford: Oxford University Press).

Sambrook, J., and Russel, D.W. (2001). Molecular Cloning: A Laboratory Manual, 3rd ed. (Cold Spring Harbor: Cold Spring Harbor Laboratory Press).

Sanders, P.M., Bui, A.Q., Weterings, K., McIntire, K.N., Hsu, Y.-C., Lee, P.Y., Truong, M.T., Beals, T.P., and Goldberg, R.B. (1999). Anther developmental defects in *Arabidopsis thaliana.* Sex. Plant Reprod. **11:** 297–322.

Schwenkert, S., Netz, D.J., Frazzon, J., Pierik, A.J., Bill, E., Gross, J., Lill, R., and Meurer, J. (2010). Chloroplast HCF101 is a scaffold protein for [4Fe-4S] cluster assembly. Biochem. J. **425:** 207–214.

Sheftel, A.D., Stehling, O., Pierik, A.J., Netz, D.J.A., Kerscher, S., Elsässer, H.-P., Wittig, I., Balk, J., Brandt, U., and Lill, R. (2009). Human ind1, an iron-sulfur cluster assembly factor for respiratory complex I. Mol. Cell. Biol. **29:** 6059–6073.

Shoffner, J.M., Lott, M.T., Lezza, A.M., Seibel, P., Ballinger, S.W., and Wallace, D.C. (1990). Myoclonic epilepsy and ragged-red fiber disease (MERRF) is associated with a mitochondrial DNA tRNA(Lys) mutation. Cell **61:** 931–937.

Swalwell, H., et al. (2011). Respiratory chain complex I deficiency caused by mitochondrial DNA mutations. Eur. J. Hum. Genet. **19:** 769–775.

Sweetlove, L.J., Taylor, N.L., and Leaver, C.J. (2007). Isolation of intact, functional mitochondria from the model plant *Arabidopsis thaliana.* Methods Mol. Biol. **372:** 125–136.

Tenisch, E.V., Lebre, A.-S., Grévent, D., de Lonlay, P., Rio, M., Zilbovicius, M., Funalot, B., Desguerre, I., Brunelle, F., Rötig, A., Munnich, A., and Boddaert, N. (2012). Massive and exclusive pontocerebellar damage in mitochondrial disease and *NUBPL* mutations. Neurology **79:** 391.

Tucker, E.J., Compton, A.G., Calvo, S.E., and Thorburn, D.R. (2011). The molecular basis of human complex I deficiency. IUBMB Life **63:** 669–677.

Tucker, E.J., Mimaki, M., Compton, A.G., McKenzie, M., Ryan, M. T., and Thorburn, D.R. (2012). Next-generation sequencing in molecular diagnosis: *NUBPL* mutations highlight the challenges of variant detection and interpretation. Hum. Mutat. **33:** 411–418.

Ugalde, C., Vogel, R., Huijbens, R., Van Den Heuvel, B., Smeitink, J., and Nijtmans, L. (2004). Human mitochondrial complex I assembles through the combination of evolutionary conserved modules: A framework to interpret complex I deficiencies. Hum. Mol. Genet. **13:** 2461–2472.

Wittig, I., Braun, H.P., and Schägger, H. (2006). Blue native PAGE. Nat. Protoc. **1:** 418–428.

Wydro, M.M., and Balk, J. (2013). Insights into the pathogenic character of a common NUBPL branch-site mutation associated with mitochondrial disease and complex I deficiency using a yeast model. Dis. Model. Mech. **6:** 1279–1284.

Zickermann, V., Kerscher, S., Zwicker, K., Tocilescu, M.A., Radermacher, M., and Brandt, U. (2009). Architecture of complex I and its implications for electron transfer and proton pumping. Biochim. Biophys. Acta **1787:** 574–583.

Zurita Rendón, O., and Shoubridge, E.A. (2012). Early complex I assembly defects result in rapid turnover of the ND1 subunit. Hum. Mol. Genet. **21:** 3815–3824.